Physics Letters B 728 (2014) 303–307

Contents lists available at ScienceDirect

Physics Letters B

www.elsevier.com/locate/physletb

Test of the $\pi g_{7/2}$ subshell closure at $Z = 58$

F. Naqvi [a,*], V. Werner [a], P. Petkov [b,c], T. Ahn [a,1], N. Cooper [a], G. Ilie [a], D. Radeck [c], C. Bernards [a], M.P. Carpenter [d], C.J. Chiara [d,e], R.V.F. Janssens [d], F.G. Kondev [d], T. Lauritsen [d], D. Seweryniak [d], Ch. Stoyanov [b], S. Zhu [d]

[a] Wright Nuclear Structure Laboratory, Yale University, New Haven, CT 06511, USA
[b] Institute for Nuclear Research and Nuclear Energy, Bulgarian Academy of Sciences, 1784 Sofia, Bulgaria
[c] Institut für Kernphysik, Universität zu Köln, 50937 Cologne, Germany
[d] Argonne National Laboratory, Argonne, IL 60439, USA
[e] Department of Chemistry and Biochemistry, University of Maryland, College Park, MD 20742, USA

ARTICLE INFO

Article history:
Received 27 September 2013
Received in revised form 2 November 2013
Accepted 25 November 2013
Available online 27 November 2013
Editor: V. Metag

Keywords:
Nuclear g factors
Lifetimes
Coulomb excitation
Angular distributions

ABSTRACT

A simultaneous lifetime and relative g-factor measurement of the 2_1^+ levels in ^{138,142}Ce was performed using the Time Dependent Recoil Into Vacuum (TDRIV) technique. The excitation mechanism was Coulomb excitation in inverse kinematics, and the experimental setup included the Yale plunger device and the Gammasphere array. The latter was used to extract angular distributions for the $2_1^+ \rightarrow 0^+$ γ-ray transitions at various target-to-stopper distances. A $g(2_1^+)$ factor of 0.26(8) for ^{138}Ce was obtained relative to the literature value of $g(2_1^+) = 0.21(5)$ in ^{142}Ce. In addition, high-precision values of the $B(\mathrm{E2}; 2_1^+ \rightarrow 0^+)$ strengths were obtained. The new data support a proposed subshell closure for the $\pi g_{7/2}$ orbital at $Z = 58$.

1. Introduction

Studying collective excitations in nuclei gives insight into the mechanisms responsible for driving these strongly interacting many-body systems toward deformation. Highly correlated collective structures originate from a coherence in the independent motion of the neutrons and protons in a mean field modified by the residual interactions between the nucleons. Investigations of isoscalar and isovector excitations in a chain of isotopes provide extensive complementary information on the proton–neutron interaction. Often, the underlying single-particle structure has been found to influence the stability of such collective excitations, showing an interesting interplay between collective and the single-particle degrees of freedom [1,2]. This competition results in an evolution of nuclear properties with N and Z, as well as with excitation energy and angular momentum.

In recent studies along the $N = 80$ ^{134}Xe [3], ^{136}Ba [4] and ^{138}Ce [5] isotones, a large impact of the single-particle structure on collective mixed-symmetry states (MSSs) was observed. In the framework of the interacting boson model-2 [6,7], MSSs are described as excitations in which protons and neutrons move partially out of phase. Their fully-symmetric analog states (FSSs), i.e., 2_1^+ states in even–even nuclei, where the two types of nucleons move in phase, have similar configurations and are lower in excitation energy. A characteristic property of MSSs is their connection to FSSs with the same number of quadrupole bosons via strong M1 transitions.

In ^{138}Ce, the M1 transition strength between the higher-lying $(2_{1,ms}^+)$ mixed-symmetry level and the first excited 2^+ state was found to be fragmented [5]. In contrast, in ^{134}Xe [3] and ^{136}Ba [4] the M1 strength remains largely concentrated in a single transition. Moreover, the total measured M1 strength is smaller for ^{138}Ce than for the other isotones. These observations were attributed to a lack of shell stabilization in ^{138}Ce [5], based on calculations within the quasiparticle–phonon-model (QPM) [8,9]. In this concept, the purity of the $2_{1,ms}^+$ state gets "washed out" in ^{138}Ce due to its single-particle structure. In a simplified independent-particle model, the complete filling of the $\pi g_{7/2}$ orbital at $Z = 58$ leads to configurations involving the higher-lying $\pi d_{5/2}$ orbital for the FS and MS one-phonon 2^+ states. Multi-phonon 2^+ states have

* Corresponding author.
E-mail address: Farheen.Naqvi@yale.edu (F. Naqvi).
[1] Present address: National Superconducting Cyclotron Laboratory, Michigan State University, East Lansing, MI 48824, USA.

0370-2693
http://dx.doi.org/10.1016/j.physletb.2013.11.057

similar proton configurations. Hence, mixing of the one-phonon MSS with nearby, higher-seniority 2^+ states can occur in ^{138}Ce, in contrast to ^{134}Xe and ^{136}Ba, where the $\pi g_{7/2}$ orbital is not fully occupied and the $2^+_{1,ms}$ state remains rather pure. Extending the shell stabilization concept to ^{140}Nd, one would expect a similar fragmentation of M1 strength as in ^{138}Ce. However, although both $2^+_{3,4} \rightarrow 2^+_1$ decays have dominant M1 character [10], only the absolute $B(\mathrm{M1}; 2^+_4 \rightarrow 2^+_1)$ strength has been measured [11], and no final conclusion can be drawn at this point.

Large-scale Shell Model (LSSM) calculations were also carried out [12] to study the evolution of MSSs in the $N = 80$ isotones. The wave functions of low-lying states in all $N = 80$ isotones up to $Z = 60$ revealed significant mixing of the $\pi g_{7/2}$ and $d_{5/2}$ configurations and no pronounced shell closure was found [12]. Additional pairing strength was needed to achieve agreement in total M1 rates. However, the fragmentation of the M1 strengths was not reproduced quantitatively. Contrary to the QPM, the LSSM predicts an isolated MSS in ^{140}Nd.

Due to the conflicting conclusions on a $\pi g_{7/2}$ subshell closure within the two models, the main components of the states in question need to be verified experimentally. The magnetic moment of a state is a sensitive probe of its wave function. Therefore, a measurement of the g factor of the 2^+_1 level in $Z = 58$, ^{138}Ce was performed for the first time using Gammasphere and the Time Dependent Recoil Into Vacuum technique (TDRIV). The 2^+_1 level in this nucleus is the fully-symmetric analog of the $2^+_{1,ms}$ state [12]. Constraining the proton–neutron contributions in the wave function of the 2^+_1 state serves as a direct test for whether enhanced pairing strength is needed in the region, which impacts the structure and purity of MSSs. In addition, the simultaneous high-precision re-measurement of $B(\mathrm{E2})\downarrow = B(\mathrm{E2}; 2^+_1 \rightarrow 0^+)$ strengths gives further insight into the existence of a possible subshell at $Z = 58$.

2. Experimental technique

Low-lying excited states in ^{138,142}Ce were populated via Coulomb excitation in inverse kinematics. ^{142}Ce and ^{138}Ce beams of intensity ∼1.7 enA and energies of 494 MeV and 480 MeV, respectively, were provided by the ATLAS accelerator at Argonne National Laboratory. The experimental setup consisted of the Yale plunger device [13] positioned at the center of the Gammasphere array [14] comprising 100 HPGe detectors arranged in 16 rings. The plunger hosted a 0.85-mg/cm^2-thick ^{24}Mg target for Coulomb excitation, followed by a ^{nat}Cu stopper of 15.7 mg/cm^2 thickness that stops the beam but allows the target recoils to pass through. The target-to-stopper distance, d_m, (relative to the point of electrical contact) was varied between ∼1 μm and 3 mm to enable a lifetime analysis of the states populated in the reaction with the Recoil Distance Doppler Shift (RDDS) method [15], as well as to measure the deorientation of the nuclear spin in vacuum. The Mg recoils were detected by a 300-mm-thick silicon detector kept at 0° with respect to the beam axis, at a distance of ∼8 mm behind the target. This detector covered a laboratory solid angle of ±29.7°. Angular distributions of deexciting γ rays were extracted at all target-to-stopper distances. A particle–γ coincidence, or a downscaled particle-singles or γ-singles event trigger, was required.

Transitions from excited states in ^{138,142}Ce are displayed in Fig. 1. The average velocities, v, of ^{138,142}Ce recoils, calculated from the observed Doppler shifts of the $2^+_1 \rightarrow 0^+$ transitions, are 5.6% and 5.8% of the velocity of light, respectively. Due to such large velocities, the Doppler-shifted components of γ transitions (SH) are well separated from the ones emitted from the nuclei at rest (US) for the detector rings with azimuthal angles less than 58°

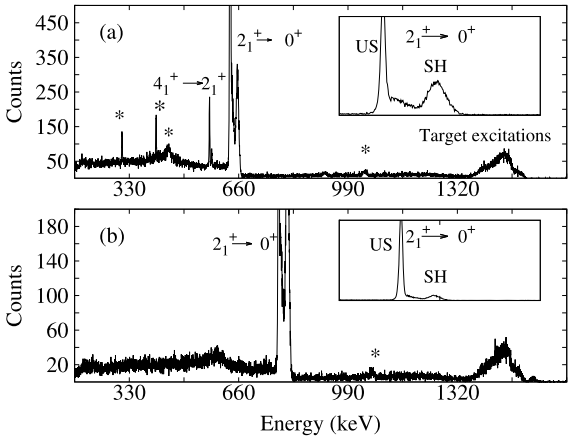

Fig. 1. Gamma-ray spectra of ^{142}Ce (a) and ^{138}Ce (b) for the target-to-stopper distances of 2 μm, 5 μm, 10 μm and 15 μm added together and measured in a forward detector ring of Gammasphere. The visible $2^+_1 \rightarrow 0^+$ and $4^+_1 \rightarrow 2^+_1$ transitions are labeled. The $2^+_1 \rightarrow 0^+$ transition originating from the excitation of the Mg target is also visible. Gamma rays marked as (*) belong to small amounts of beam contaminants and background.

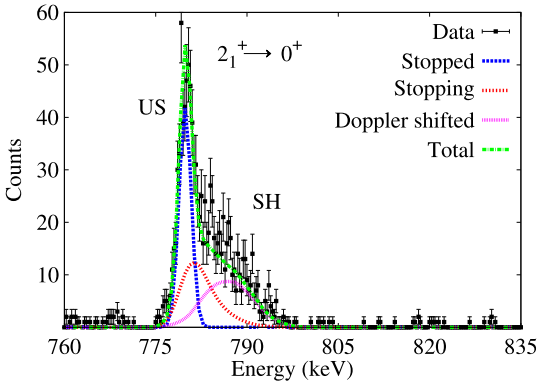

Fig. 2. Gamma-ray spectrum from ^{138}Ce for a detector ring at 79.2°. Monte Carlo simulations for different components are shown with dashed lines.

and greater than 122° with respect to the beam axis (see insets in Fig. 1). For angles near 90°, Monte Carlo simulations were used to estimate the centroids and shapes of SH and US components. The Monte Carlo code [16,17] simulates the time behavior of the velocity of the ions of interest in three dimensions. It takes into account the reaction kinematics, the slowing down in the target and stopper, and the free flight in vacuum. Details about the determination of stopping powers can be found in Ref. [18]. A γ-ray spectrum for the 79.2° detector ring is compared in Fig. 2 to the Monte Carlo simulations fitting the relative heights of the various peak components. A more detailed description of a similar analysis, including the fit of the stopping component at forward and backward angles is provided in Refs. [19,20].

3. Results

The angular distributions of the $2^+_1 \rightarrow 0^+$ transitions are described by the standard formalism [21] for perturbed particle–γ correlations as

$$W(t, \theta_\gamma) = \sum_{k=0,2,4} Q_k B_k R_k G_k(t) P_k\big(\cos(\theta_\gamma)\big), \qquad (1)$$

where the Q_k coefficients take into account the attenuation due to the finite solid angle of the Ge detectors [22], B_k are the m state distribution coefficients, R_k are the Racah coefficients [21],

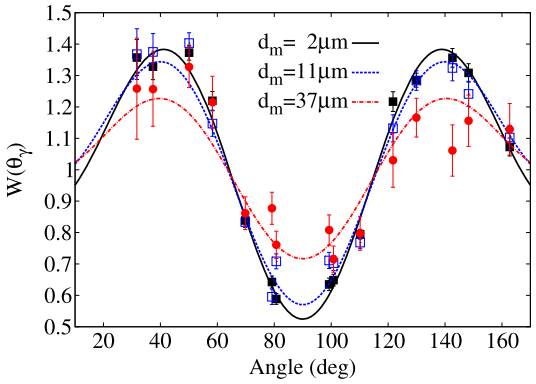

Fig. 3. Normalized angular distribution curves for the unshifted component of the $2_1^+ \rightarrow 0^+$ transition in ^{138}Ce at different measured distances, d_m, between target and stopper.

$P_k(\cos(\theta_\gamma))$ are the associated Legendre polynomials, and $G_k(t)$ are the time-dependent vacuum attenuation coefficients, first introduced on the basis of the theory of Abragam and Pound [23].

As the nuclei emerge from the target, a loss of alignment of the nuclear spin is observed due to hyperfine interactions. The resulting reduction in the anisotropy of the particle–γ angular correlations is represented by the $G_k(t)$ factor in Eq. (1). According to the static approach discussed in Refs. [19,24–28], requiring the electronic lifetimes to be considerably larger than the average lifetime of the nuclear state, the deorientation coefficients $G_k(t)$ are related to the g factor of the state by

$$G_k(t) = \alpha_k + (1-\alpha_k)e^{-\Gamma_k t}; \qquad \Gamma_k = \frac{|g|}{C_k}. \tag{2}$$

Herein, the α_k coefficients define the anisotropy of the γ angular distribution at $t \rightarrow \infty$ [29] and C_k are the hyperfine interaction parameters, which can be calibrated from a known g factor of a state in the same isotopic chain [24]. Using the TDRIV technique, relative g factors are obtained, and in this experiment, the known $g(2_1^+) = 0.21(5)$ factor in ^{142}Ce [30] served as a reference value. Identical beam characteristics for ^{138,142}Ce were maintained, resulting in similar charge state distributions and hyperfine interaction strengths after Coulomb excitation. Particle-γ angular correlations as a function of time were obtained by varying the target-to-stopper distance. Normalized γ-ray angular distributions measured for the unshifted components of the $2_1^+ \rightarrow 0^+$ transition in ^{138}Ce at different distances are presented in Fig. 3. A relativistic Lorentz-boost factor for the solid angle was introduced to correct the intensities of Doppler-shifted γ rays [31]. The degree of isotropy of the angular distributions increases with distance. This is a clear indication of deorientation due to the hyperfine interactions. To extract the $G_k(t)$ coefficients, the normalized experimental angular distribution curves were fitted to the function

$$W(t,\theta_\gamma) = 1 + \sum_{k=2,4} A_k(t) P_k\big(\cos(\theta_\gamma)\big), \tag{3}$$

where $A_k(t) = Q_k B_k R_k G_k(t)$. The Coulomb excitation code of Winther and De Boer [32] provided the statistical tensors, ρ_k, required to calculate the B_k coefficients. For the unshifted component of the transition, the time t for deorientation is defined by the target-to-stopper distance, while, for the shifted one, time varies in the interval $[0, d/v]$. As shown in [19], the in-flight deorientation coefficients take into account the decay of the state and are given by

$$\tilde{G}_k(t) = \frac{\int_0^t e^{-\lambda t}\{\alpha_k + (1-\alpha_k)e^{-\Gamma_k t}\}\,dt}{\int_0^t e^{-\lambda t}\,dt}, \tag{4}$$

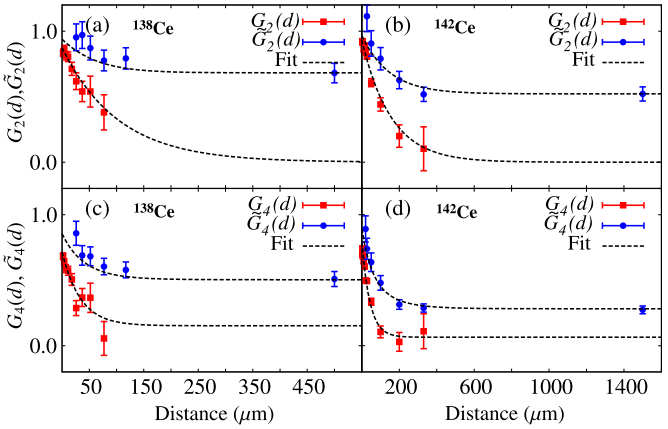

Fig. 4. The experimental deorientation coefficients, $G_{2,4}$ and $\tilde{G}_{2,4}$ ((a), (c)) extracted from the unshifted and shifted components, respectively, of $2_1^+ \rightarrow 0^+$ transitions in ^{138}Ce. The corresponding coefficients for ^{142}Ce are shown in (b), (d).

where λ is the decay constant. The deorientation coefficients for ^{138,142}Ce and for $k = 2, 4$, are displayed in Fig. 4.

To obtain the g factor of a nuclear state from the experimentally-deduced deorientation coefficients, the level lifetime, τ, is required. As a first estimate, the literature values for the 2_1^+ states in ^{138,142}Ce [30] were adopted. The resulting deorientation coefficients were fed back into a separate lifetime analysis described below in an iterative approach until convergence was achieved. Lifetimes were obtained via the RDDS method [15]. The ratios of the shifted intensities, I_{SH}, corrected for the Lorentz boost and deorientation, to the total intensities, $P = I_{SH}/(I_{SH} + I_{US})$ are plotted as a function of distance in Fig. 5. A single exponential decay function of the form $P(d) = 1 - \exp(-\lambda d/v)$ was fitted to the data to obtain the lifetime of the 2_1^+ level in ^{138}Ce. In the equation above, $d = d_m + d_0$, with d_m being the measured distance between the target and the stopper, and d_0 is the offset, corresponding to the minimum achievable distance without electrical contact. Independent fits from 16 detector rings resulted in a precise determination of this offset, which was then fed into the fit of deorientation data. In ^{138}Ce, the population of higher-lying states is negligible (see Fig. 1). The 4_1^+ state at 1477 keV is populated with an approximate 1% probability with respect to the 2_1^+ level. The observed $4_1^+ \rightarrow 2_1^+$ transition has a dominant Doppler-shifted component, even for the smallest, 2 μm, target-to-stopper distance. Considering the velocity of the ^{138}Ce recoils, and the total flight distance including the 13 μm offset, a lifetime of less than 1 ps was estimated for the 4_1^+ state. The effect of this feeding on the intrinsic lifetime of the 2_1^+ state in ^{138}Ce is less than 1% and is included in the adopted uncertainty. In ^{142}Ce, a feeding correction from the higher-lying 4_1^+ level with a lifetime of 10.8(10) ps [30] had to be considered. The decay probability curve for this nucleus was fitted with a combined exponential decay function of the form

$$P(d) = P_0\big(1 - e^{\frac{-\lambda_0 d}{v}}\big) + P_1\left(1 - \frac{\lambda_1 e^{\frac{-\lambda_0 d}{v}} - \lambda_0 e^{\frac{-\lambda_1 d}{v}}}{\lambda_1 - \lambda_0}\right). \tag{5}$$

Here, P_0, λ_0 and P_1, λ_1 are the respective population probabilities and decay constants of the 2_1^+ and 4_1^+ states. For ^{142}Ce, P_0 was 97% and P_1 3%, as given by the Winther–De Boer code [32]. These numbers were verified by the measured $4_1^+ \rightarrow 2_1^+$ and $2_1^+ \rightarrow 0^+$ intensities. Lifetimes were obtained for the 16 detector rings and the weighted averages are adopted in Table 1 in comparison to literature values, along with the extracted $B(E2)\downarrow$ values for ^{138,142}Ce. The present results are in good agreement with previous measurements and present a significant improvement in the

Table 1
Parameters from simultaneous fits of the experimental deorientation parameters for ^{138,142}Ce, see text for details.

Isotope	α_2	Γ_2	α_4	Γ_4	τ (ps)		B(E2)↓ W.u.
					This work	Literature [30]	
^{142}Ce	<0.18	0.11(3)	0.06(4)	0.40(3)	8.19(9)[a]	8.02(17)	20.98(23)[b]
^{138}Ce	<0.43	0.16(8)	0.15(10)	0.50(10)	2.84(6)[a]	2.97(20)	22.32(31)[b]

[a] Adopted values are the weighted average of 16 rings of Gammasphere.
[b] Extracted from the measured lifetime of the 2_1^+ level.

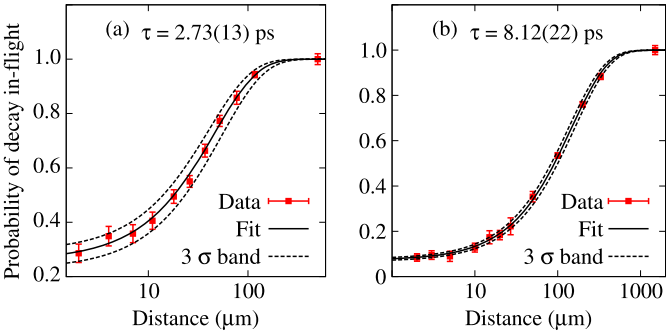

Fig. 5. Probability of in-flight decay as a function of target-to-stopper distance for ^{138}Ce (a) and ^{142}Ce (b). Data and lifetime from a forward detector ring at an azimuthal angle of 37.4° are presented.

precision, especially for ^{138}Ce. To extract the α_k and Γ_k factors, the experimental deorientation coefficients for shifted and unshifted components were fitted simultaneously with Eqs. (2) and (4). Only data points where significant numbers of counts were observed in the respective peaks were included. The resulting deorientation coefficients are listed in Table 1. The obtained α_2 coefficients are close to zero with a large uncertainty for both the Ce isotopes, therefore only upper bounds are provided. The weighted average of the ratio, $\frac{\Gamma_k(^{138}\mathrm{Ce})}{\Gamma_k(^{142}\mathrm{Ce})}$ is 1.25(24) resulting in an absolute value of the relative g factor of the 2_1^+ state in ^{138}Ce of 0.26(5)(6). The first error is statistical while the second is inherited from the existing ^{142}Ce g factor [30]. The short lifetime of the 2_1^+ level in ^{138}Ce posed a challenge for observing the deorientation of the angular distributions. However, this Letter reports the first measurement of an unknown g factor using the TDRIV technique in combination with Gammasphere. Only the large angular coverage and granularity of the array enabled the observation of this small effect. In view of the remaining large uncertainty, an absolute g-factor measurement using the transient-field technique should be performed on ^{142}Ce, where higher precision can be achieved due to the longer lifetime of the 2_1^+ state.

4. Discussion

Assuming a positive sign for the $g(2_1^+)$ factor in ^{138}Ce, the result is a direct test of the wave function of the state. Hence, the new data contribute to the recent discussion on the $\pi g_{7/2}$ subshell closure. In the following, the B(E2)↓ strength and the new experimental value of $g(2_1^+)$ factor in ^{138}Ce are compared to predictions of the QPM and LSSM calculations [see Fig. 6(a, b)].

The g factors calculated within the QPM drop toward $Z = 58$, in accordance with a decreasing importance of proton contributions to the 2_1^+ wave function, in the presence of a $\pi g_{7/2}$ subshell closure [see Fig. 6(b)]. Data up to $Z = 56$ suggest rather constant $g(2_1^+)$ factors, in fair agreement with the QPM. The present result at $Z = 58$ does support a drop, however, a near-constant behavior cannot be ruled out in view of the uncertainty for the measured value. A constant trend of the $g(2_1^+)$ factors would be expected

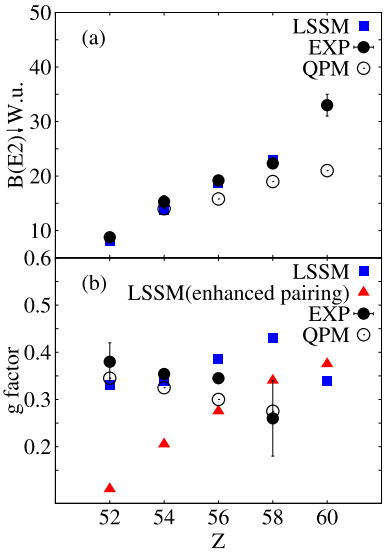

Fig. 6. QPM and LSSM [12] predictions for the B(E2)↓ (a) and g factor (b) of the 2_1^+ states in the $N = 80$ isotones. The corresponding experimental values are shown for comparison.

for rather pure $\pi g_{7/2}^{2\sigma}$ ($\sigma = 1, 2, 3$) configurations, until $Z = 58$ is reached. Similarly, the experimental B(E2)↓ values are reproduced well by QPM for $Z < 60$. However, a sudden rise in B(E2) strength for Nd is not predicted by the model.

The new data discriminate between two LSSM predictions by the Strasbourg group [12] for ^{138}Ce. The first used the GCN5082 interaction, derived from a realistic nucleon–nucleon Bonn-C potential within the *gdsh* valence space, and the second was obtained after modifying the pairing matrix elements of the same interaction. The two calculations led to significantly different results for g factors. As seen in Fig. 6(b), the result from the original interaction is excluded by the measurement by more than 2σ, whereas the prediction with enhanced pairing lies within the present error bar. Hence, modifications in the pairing interaction, as applied to the GCN5082 interaction, appear to be necessary for a good description of the nuclear wave functions at $Z = 58$. In contrast, when considering also the ^{132}Te [24], ^{134}Xe [33] and ^{136}Ba [34] isotones, the recent data are markedly different from the predictions of the interaction with enhanced pairing. The original GCN5082 interaction appears to reproduce the observations better below Ce. This may indicate that an enhanced pairing interaction is of higher importance at $Z = 58$, where the $\pi g_{7/2}$ orbital is filled.

In recent work on ^{140}Nd [35], a modest suppression of the B(E2)↓ strength at $Z = 58$ had been discussed as a signature of the subshell closure at $Z = 58$. However, the literature B(E2)↓ value had an error bar of about 8%. In the present TDRIV experiment, level lifetimes are obtained with high precision, and the statistical error is reduced to about 1.5%. The deviation from a near-linear trend in B(E2)↓ values pointed out in Ref. [35] is now confirmed and the new B(E2)↓ value in ^{138}Ce agrees well with the LSSM prediction, similar to that observed for the lower-Z isotones.

To summarize, the $g(2_1^+)$ factor in ^{138}Ce was measured relative to that in ^{142}Ce employing the TDRIV technique in inverse-kinematics Coulomb excitation. The resulting value is in good agreement with a LSSM calculation explicitly modifying pairing matrix elements. The measured $B(\mathrm{E2})\downarrow$ value in ^{138}Ce supports a subshell closure at $Z = 58$. These results underline the conclusion from Ref. [12] that the pairing interaction is important for a correct understanding of proton–neutron symmetry in low-lying collective states at $Z = 58$. In order to differentiate between, and to give stronger constraints to QPM and LSSM calculations, the reference $g(2_1^+)$ factor in ^{142}Ce should be remeasured with higher precision.

Acknowledgements

This work is supported by the U.S. DOE, Office of Nuclear Physics, under Grant No. DE-FG02-91ER-40609 and Contract No. DE-AC02-06CH11357. The support of Bulgarian Science Foundation under Contract No. DFNI-E 01/2 and NuPNET-SARFEN ДНС7РП01/0003 is appreciated. Ch.S. acknowledges support by the DAAD German–Bulgarian exchange program under Grant Nos. PPP 50751591 and DNTS/01/2/2011. Discussions with A. Stuchbery are acknowledged. The authors are indebted to the ATLAS staff for providing excellent beam conditions.

References

[1] A. Richter, Prog. Part. Nucl. Phys. 34 (1995) 261.
[2] N. Pietralla, P. von Brentano, A. Lisetskiy, Prog. Part. Nucl. Phys. 60 (2008) 225.
[3] T. Ahn, et al., Phys. Lett. B 679 (2009) 19.
[4] N. Pietralla, et al., Phys. Rev. C 64 (2001) 031301.
[5] G. Rainovski, et al., Phys. Rev. Lett. 96 (2006) 122501.
[6] A. Arima, F. Iachello, Phys. Rev. Lett. 35 (1975) 1069.
[7] F. Iachello, A. Arima, The Interacting Boson Model, Cambridge University Press, Cambridge, 1987.
[8] N. Lo Iudice, V.Yu. Ponomarev, Ch. Stoyanov, A.V. Sushkov, V.V. Voronov, J. Phys. G, Nucl. Part. Phys. 39 (2012) 043101.
[9] N. Lo Iudice, Ch. Stoyanov, D. Tarpanov, Phys. Rev. C 77 (2008) 044310.
[10] E. Williams, et al., Phys. Rev. C 80 (2009) 054309.
[11] K.A. Gladinski, et al., Phys. Rev. C 82 (2010) 037302.
[12] K. Sieja, G. Martinez-Pinedo, L. Coquard, N. Pietralla, Phys. Rev. C 80 (2009) 054311.
[13] R. Krücken, J. Res. Natl. Inst. Stand. Technol. 105 (2000) 53.
[14] I.Y. Lee, Nucl. Phys. A 520 (1990) c641.
[15] T.K. Alexander, J.S. Forster, in: M. Baranger, E. Vogt (Eds.), Advances in Nuclear Physics, vol. 10, Plenum Press, New York, 1978, p. 197.
[16] P. Petkov, et al., Nucl. Instrum. Methods Phys. Res. A 431 (1999) 208.
[17] P. Petkov, et al., Nucl. Phys. A 674 (2000) 357.
[18] P. Petkov, et al., Nucl. Phys. A 640 (1998) 293.
[19] D. Radeck, et al., Phys. Rev. C 85 (2012) 014301.
[20] D. Radeck, PhD Thesis, University of Cologne, ISBN 9783843909907, 2012.
[21] H.J. Rose, D.M. Brink, Rev. Mod. Phys. 39 (1967) 306.
[22] J. Barrete, G. Lamoureux, S. Monaro, Nucl. Instrum. Methods 93 (1971) 1.
[23] A. Abragam, R. Pound, Phys. Rev. 92 (1953) 943.
[24] A.E. Stuchbery, N.J. Stone, Phys. Rev. C 76 (2007) 034307.
[25] H.R. Andrews, R.L. Graham, et al., Hyperfine Interact. 4 (1978) 110.
[26] G. Goldring, in: R. Bock (Ed.), Heavy Ion Collisions, vol. 3, North-Holland Publishing Company, Amsterdam, 1982.
[27] J. Billowes, Hyperfine Interact. 30 (1986) 265.
[28] G. Goldring, K. Hagmeyer, et al., Hyperfine Interact. 5 (1977) 283.
[29] R. Nordhagen, in: G. Goldring, R. Kailash (Eds.), Hyperfine Interactions in Excited Nuclei, vol. 3, Gordon and Breach, New York, 1971.
[30] http://www.nndc.bnl.gov/ensdf.
[31] D. Pelte, D. Schwalm, in: R. Bock (Ed.), Heavy Ion Collision, vol. 3, North-Holland Publishing company, Amsterdam, 1982.
[32] A. Winther, J. De Boer, in: K. Alder, A. Winther (Eds.), Perspective in Physics Series: Coulomb Excitation, Academic Press, New York, 1966.
[33] G. Jakob, et al., Phys. Rev. C 65 (2002) 024316.
[34] J.M. Brennan, M. Hass, N.K.B. Shu, N. Benczer-Koller, Phys. Rev. C 21 (1980) 574.
[35] C. Bauer, et al., Phys. Rev. C 88 (2013) 021302.